Utveckling av processteg för återvinning av litium från uttjänta litiumjonbatterier

Development of Process Steps for Recovery of Lithium from spent Lithium-ion Batteries

Granted Application 20-508

Lena Sundqvist Öqvist

Final report with contributions from

Faizan Muneer

Moses Charles Siame

Anton Andersson

Safoura Babanejad

Summary

I **WP1**, mineral processing for separating graphite and fluorine (F) from lithium (Li) and the transition metals in black mass (BM) after thermal treatment ranging from 400-1200°C in air and inert atmosphere showed difficulties to remove both graphite and fluorine efficiently. Cu was distributed to the coarsest fraction (>425 µm) after thermal treatment at 670°C in inert and 720°C in air atmosphere, a fraction which is proposed to be separated by gravimetrical unit operations. Cobalt (Co), nickel (Ni), manganese (Mn), and Li are mainly distributed in the two finest fractions together with graphite and F, which, are deemed to require surface-specific unit operations such as flotation for separation. BM thermally treated at 720°C in air was the most promising material from an industrial perspective as 67 % of all F was removed while all Li remained in the sample.

In **WP2** the evaporation of Li and F from synthetic slags designed for finding the conditions of maximum Li evaporation. In inert atmosphere without reducing agents the Li evaporation reaches a maximum of ~40% of initial compared to 68% in the EAF trials.[13] The lab tests indicate that higher initial Al_2O_3 content and basicity promote the evaporation. A larger part of F evaporated in the Tamman furnace tests compared to in the vertical tube furnace (VTF) tests, but the amount directed to the gas was always lower than thermodynamically estimated, which indicate kinetic limitations. The thermodynamic calculations considering interaction with a MgO crucible indicate that F is crucial for evaporation as it occurs through LiF, $(LiF)_2$ and $(LiF)_3$ under inert conditions. In BM smelting reduction by graphite may enable evaporation of metallic Li, which may form Li_2CO_3 (dominating Li compound in the EAF dust) in the oxidizing conditions with CO_2 present in the off-gas duct. Further optimization of the slag can enhance the evaporation and decrease the kinetic limitations. Fluorides flux the slag at 750°C, at 1500°C when a considerable part of F has evaporated the slag mainly consists of oxides. F containing compounds in the slag may contribute to lower viscosity, which enhances mass transfer in the slag.

The melting tests in **WP3** used the most promising slag composition for Li evaporation defined in WP1. BM thermally treated at 720°C in air was utilized. Dust shortage in the laboratory tests led to using pilot-scale dust from EAF smelting for leaching tests in WP4. Transition metals report to the metallic phase, indicating that this slag composition won't hinder valuable metals recycling. Li is found in the dust and can be hydro metallurgically recovered. Despite design for Li evaporation, LA-ICP-MS analyses shows significant Li content in the slag. Inert conditions contribute to LiF in the dust, Li_2CO_3 likely forms when reduced and evaporated metallic Li reacts with CO_2-rich off-gas at high oxygen potential.

In **WP4** it was stated that the dust produced in pilot scale tests contained around 65.2 % of Li_2CO_3 and 7.22 % of LiF. The highest leaching recovery achieved for leaching in carbonated or lime water was 70% and 77%, respectively. This indicates a potential inhibition of the dissolution also indicated by the SEM evaluation of leach residue. Acetone and isopropanol were selected as possible antisolvent for $LiOH{\cdot}H_2O$ crystallization of Li leached by lime milk. The optimal organic/aqueous ratio for crystallization was 4 for acetone and 5 for iso propanol crystallising 93% and 76% of the Li. Further optimisation for lower co-crystallisation of impurities is planned.

WP5 focuses on the potential contribution of findings to meet battery regulations. To achieve a 70% overall recycling rate for LIBs, recovering Li and a major portion of graphite is necessary. Thermal treatment followed by physical separation can improve BM quality for smelting. After treatment at 670°C in inert and 720°C in air, Cu was concentrated in a coarse fraction (> 425 µm), separable by gravimetric methods. Graphite was found in finer fractions (38-100 µm and < 38 µm), along with Co, Ni, Mn, and Li. Flotation could possibly separate graphite and metal-containing phases in these fractions. In the studied process, Co, Ni, and Mn yields were 98.2%, 98.4%, and 91.5%, respectively.

In pilot-scale tests, 68% of Li was directed to the dust, with up to 77% recovery in lime milk leaching. 93% of leached Li was recovered as $LiOH{\cdot}H_2O$ in antisolvent crystallization, yielding an overall Li

recovery of 49%. Further optimization to increase Li directed to the dust, particularly in the form of more easily leachable Li_2CO_3, is feasible through slag modification and control of reducing conditions.

Contents

Summary 2

1 Introduction 4

1.1 Background 4

2 Conducted work and results 5

2.1 WP1 Mineral processing separation of carbon from black mass (AP1: Mineralteknisk separation av kol från batterimassa). 5

2.1.1 Materials 5

2.1.2 Methods 5

2.1.3 Results and discussion WP1 6

2.1.4 Summary of WP1 10

2.2 WP2 Mapping of Li capacity in slag, and evaporation of Li from slag as function of slag composition, temperature and gas stirring (AP2: Kartläggning av Li-kapacitet i slagg och Li-förångning från slagg som funktion av slaggsammansättning, temperatur och gasomrörning). 10

2.2.1 Material and methods 11

2.2.2 Results of melting tests in WP2 13

2.2.3 Summarized discussion of WP2 results 14

2.3 WP3 optimization of Li distribution to dust with sustained quality of metal alloy and possible recovery of slag. (AP3: Optimering av fördelning av Li till stoft med bibehållen kvalitet av metallegering och möjlig återvinning av slagg) 15

2.3.1 Material and methods in WP3 15

2.3.2 Results and discussion 17

2.3.3 Summary of WP 3 19

2.4 WP4 Process improvement for dissolution and extraction of Li in dust formed in the melting process. (AP4: Processförbättring för upplösning och extraktion av Li från lösning för återvinning av Li från stoftet bildat vid smältprocessen) 20

2.4.1 Materials and methods 20

2.4.2 Results and discussion of WP4 21

2.5 WP5 Techno-economical assessment of proposed process (AP5: Teknoekonomisk analys kopplat till den föreslagna processen.) 23

2.5.1 Studied process steps relative state-of the art and battery regulation 23

3 References 25

1 Introduction

1.1 Background

The utilization of Li-ion batteries (Li-ion batteries, LIBs) in the automotive industry has surpassed the electronics market and to establish Li-ion battery recycling in Sweden it is important to establish knowledge in the field.[1]. Statistical data from the U.S. Geological Survey shows that the percentage of the total extracted lithium (Li) being utilized in the battery industry has increased from 7 % to 48 % going from 1994 to 2017 [2][3]. In a study published in 2016, Choubey et al. [4] presented that the trend in market share and increased purchases of electrified vehicles projects a 1.5-fold increase in demand for lithium carbonate (Li_2CO_3) equivalents (LCE) from 2015 to 2025[4] or a demand increasing from 265,000 to 398,000 LCE[4]. Newer projections illustrate the vast growth in the field of utilization of LIBs in electric vehicles (EV). For example, the European Union (EU) estimated that the number of EV will increase from four million in 2018 to 50-200 million in 2028, reaching 900 million EV in 2048.

The increased demand and production volumes of EVs increase the volumes of end-of-life batteries entering the recycling processes shortly after the increased production volumes as the cell of the LIBs has an average life span of one to three years[5]. Liu et al.[6] summarized the current status of the commercial recycling processes treating spent LIBs. The field is moving forward quickly; however, when published, the pyro-dominant recycling processes exceeded the hydro-dominant in number and capacity[6]. Makuza et al.25[7] compared the hydro- and pyrometallurgical recycling processes for LIBs. The established pyrometallurgical processes has high reaction rates, high throughput, greater flexibility in feedstock, simple operation, and low environmental impact of the generated residues[7], but focuses mainly focuses on the metals of higher value, and Li is lost to the slag or to the dust. To reach the high ambitions of a total recycling of 70% of the Li-ion battery as well as 95% recovery of cobalt (Co), nickel (Ni) and copper (Cu) and 70% recovery of Li, there is need for development of existing processes. Further, will require

This project focuses on the development of process steps to meet five defined challenges (C1-C5) limiting the recovery rates of the Li-ion batteries that can be shortly summarized as

C1: High graphite and F content that disturb smelting and hydrometallurgical processes

C2: Knowledge on how to efficiently control the distribution of Li to the dust for hydrometallurgical recovery.

C3: Maintained quality of generated metal alloy with value metal for recovery

C4: Knowledge on which compounds that will be directed to the dust, including F-containing ones and how this will influence the recovery of Li.

C5: Knowledge on the techno-economic aspects of new process

2 Conducted work and results

2.1 WP1 Mineral processing separation of carbon from black mass (AP1: Mineralteknisk separation av kol från batterimassa).

2.1.1 Materials

The BM from AkkuSer Oy was prepared by crushing batteries of NMC 1:1:1 type, magnetic separation of iron and screening at 1 mm producing two fractions. In the present study, the finest fraction rich in Co, Ni, Mn, Li, and graphite, representing 59% of the material, was used. Sample splitting was done by a Jones riffler to get representative samples for experiments and analysis. Samples for analyses were split after grinding in a ring mill to prevent larger particles of specific components from dominating in a given sample. The original non-treated BM, as well as BM from each thermal treatment, were sieved using a W.S. Tyler RO-Tap sieve shaker in a stack with sieves of 38, 53, 75, 100, 150, 212, 425, 600, 840, 1190, and 1680 µm. Four fractions, >425, 100-425, 38-100, and <38 µm, corresponding to approximately 25 % of mass were analyzed.

2.1.2 Methods

2.1.2.1 Thermogravimetric Analyses and Therma l treatment

The mass loss upon heating in inert and synthetic air atmospheres was studied in thermogravimetric analysis (TGA) using a Setaram Setsys Evolution TG-DSC equipment. Prior to the tests, the buoyancy effect of the gas on an inert sample of Al_2O_3 was determined. This effect was accounted for in the subsequent tests on the BM sample. The experiments were performed in N_2 and synthetic air (80 vol.% N_2 and 20 vol.% O_2) of a total gas flow of 50 $mLmin^{-1}$ in an Al_2O_3 crucible. The samples of 14.595 and 15.570 mg were heated from ambient temperature to 1200°C at a heating rate of 5°$Cmin^{-1}$.

Based on the TGA tests the temperatures selected for the thermal treatment of around 300 g of sample in air atmosphere were 400, 530, 720, and 1200°C and in inert atmosphere 420, 670, 790, and 1200°C using an Entech muffle furnace and Ruhstrat resistance heating furnace, respectively. Air was supplied via the natural draft in the furnace. For inert atmosphere the furnace was flushed with Ar before starting the test under inert atmosphere.

2.1.2.2 Characterization of Samples

Table 1. Analytical methods used for samples characterization. N.A. denotes not applicable. Whole denotes the sample that has not been fractionated, and fractions denote that the four different fractions.

Information	Original sample		Air atmosphere					Inert atmosphere					
Temp. [°C]	N.A.	N.A.	400	530	720	720	1200	420	670	670	790	1200	1200
Whole sample	X		X	X	X		X	X	X		X	X	
Fractions		X				X				X			X
ICP-SFMS	X	X	X	X	X	X		X	X	X	X	X	X
F analysis	X	X	X	X	X	X		X	X	X	X	X	X
C separation	X		X	X	X			X	X		X	X	
Total C	X	X	X	X	X	X		X	X	X	X	X	X
XRD	X	X	X	X	X	X		X	X	X	X	X	X
SEM-EDS	X		X	X	X			X	X		X	X	

The analyzes performed on the different samples generated in the thermal treatment and fractionation are summarized in **Table 1**. In addition, all samples, including all fractionated samples, were analyzed for their density using a Micromeritics AccuPyc II 1340 helium gas displacement pycnometer.

The Cu, Co, Li, Mn, and Ni content were analyzed with inductively coupled plasma sector field mass spectrometry (ICP-SFMS) in a Thermo Finnigan Element 1 ICP-SFMS unit on samples microwave-assisted digested in a mixture of HF, HCl, and HNO_3. The F content in the samples was analyzed using the F ion-selective electrode method in accordance with the United States Environmental Protection

Agency Method 9214. The carbon separation analyses were performed to determine the total C content as well as the distribution of organic C and graphite. The analyses were performed with LECO equipment RC612 and CS444 using the standards ASTM D7582 and ASTM E1019.

The mineralogical composition was determined using X-ray diffraction (XRD) using a Panalytical Empyrean XRD unit operating with Cu K_α (generated at 45 kV and 40mA). Furthermore, in order to aid the phase identification, selected samples were analyzed using scanning electron microscopy with energy-dispersive X-ray spectroscopy (SEM-EDS). The SEM-EDS analyses were performed with a Gemini Zeiss Merlin field emission SEM (FE-SEM) with an Oxford Instruments Xmax silicon drift EDS detector.

2.1.3 Results and discussion WP1

2.1.3.1 Characterization of the Original Sample

Table 2 presents the chemical composition of the original sample. The carbon fractionation suggests presence of a considerable amount of plastic material, although a coarse fraction was separated during the processing of the battery cells. Several elements provide indications of the presence of phases, e.g., P suggests $LiPF_6$, and F suggests polyvinylidene fluoride (PVDF). Elements associated with the active cathode material, current collectors and anode materials were present in significant amounts as well.

Table 2 Chemical composition of the original sample of the BM presented in wt.%.

Element	Concentration [wt.%]	Method
Li	2.87	ICP-SFMS
$C_{organic}$	17.40	LECO
$C_{inorganic}$	12.50	LECO
F	3.59	Potentiometric
Al	3.77	XRF
Si	0.23	XRF
P	0.86	XRF
Mn	6.04	ICP-SFMS
Fe	0.18	ICP-SFMS
Co	9.59	ICP-SFMS
Ni	7.59	ICP-SFMS
Cu	7.17	ICP-SFMS

Based on XRD and SEM analysis the phase distribution in the sample was estimated, see **Table 3**. Some phase could not be detected due to analytical limitations but indirectly deduced through calculations and using the results from TGA.

Table 3 Estimated phase distribution based on the chemical analysis, XRD and SEM-EDS analyses.

Phase	Mass distribution [%]
$LiPF_6$	4.83
$(C_2H_2F_2)_n$	0.82
$(C_2H_4)_n$	22.89
C	14.30
Cu	8.20
Al	4.31
$LiNi_{0.33}Mn_{0.33}Co_{0.33}O_2$	44.64
Total	100.0

2.1.3.2 Deciding Points of Interest for Thermal Treatment

The information regarding the phase composition was combined with previously published data to understand the results from the TGA experiments. As stated, the plastic component was unknown and, therefore, data on both PE and PP were considered. The decomposition during non-isothermal pyrolysis of LDPE and HDPE has been shown to start at 387-422°C and finish at 481-502°C[8]. These results are consistent with those of other researchers[9][10]and, therefore, PE present in the BM of the current study should decompose before reaching the chosen temperature of 670°C. In comparison, non-isothermal combustion of PE has been shown to occur within the temperature range of 423 to 436°C[11], which is

consistent with the achieved mass loss. The theoretical mass loss related to the molecule of $LiNi_{0.33}Mn_{0.33}Co_{0.33}O_2$ is 40.4 % if Li evaporates and 33.2 % if Li stays in the sample. The total mass loss in the BM is consistent with this.

2.1.3.3 Effect of Thermal Treatment on Chemical and Mineralogical Composition

The mass loss of the TGA and thermal treatment is shown in **Table 4**, significant differences observed are possibly an effect of the larger sample size, which may pose limitations in reaching the same mass loss as for the very small sample used in the TGA.

Table 4 Comparison of residual mass [%] after TGA and thermal treatment (TT).

Air			Inert		
Temp. [°C]	TGA [%]	TT [%]	Temp. [°C]	TGA [%]	TT [%]
400	88.4	85.7	420	91.2	87.8
530	68.3	83.7	670	87.0	81.8
720	64.8	79.8	790	77.1	80.2
1200	59.9	78.2	1200	46.4	71.5

Elements such as $C_{organic}$, $C_{inorganic}$, F, and Li that may either evaporate as is or form volatile compounds upon reactions were analyzed. Li remained in all samples except the one treated at 1200°C. In terms of F, a larger portion was evaporated from the sample at the lowest temperatures in both atmospheres. The $C_{organic}$ was partially combusted or pyrolyzed at all temperatures, but the $C_{inorganic}$ remained. Changes in mineralogical, or phase, composition upon thermal treatment were studied using XRD and SEM-EDS. Since possible phases had overlapping peak positions in the diffractogram, a combination of both analytical techniques was required.

Comparing the XRD measurements of the original sample and the sample thermally treated in inert atmosphere at 420°C, no changes were observed. Based on all characterization made some pyrolysis of the organic components and partial reduction of the $Li_3Ni_{0.33}Mn_{0.33}Co_{0.33}O_2$ was found. Increasing the temperature to 670°C facilitates the complete decomposition of $Li_3Ni_{0.33}Mn_{0.33}Co_{0.33}O_2$, forming metallic Ni and a metal oxide. From a thermodynamic standpoint, Ni should be reduced first, see **Figure 1**, followed by Co and Mn but by comparing to data at 790°C it can be seen that the reduction to Ni was incomplete at 670°C and part of the Ni was present in the (Ni, Mn, Co)O solid solution. The solid solution is complete throughout the whole compositional region. Li from $Li_3Ni_{0.33}Mn_{0.33}Co_{0.33}O_2$ is suggested to be distributed between $LiAlO_2$ and LiF, but overlapping peaks makes the XRD evaluation challenging. Particles analyzed for 100% F in SEM-EDS is likely LiF and spectrums suggesting an atomic ratio 1:2 for Al:O were found in connection to the unreacted Al core indicating Al acting as a reductant. Cu was not reacted in the thermal treatment at 670°C and graphite was still present in the sample, although both Ni and Co can be reduced by C from a thermodynamic standpoint. Possibly, the reaction rates are negligible at the present temperature. The increase of temperature from 670 to 790°C, did not give any new phases further reduction of Ni in the MeO solid solution occurred. Unreacted Al was found in the SEM-EDS analyses, but the $LiAlO_2$ could be determined by XRD.

Thermally treating the BM at 1200°C in inert atmosphere caused melting of Cu (melting point of 1085°C) and the subsequent formation of a solution containing Cu, Ni, Mn, and Co. After cooling, the solid solution was found in the form of droplets. Al had been consumed as a reducing agent in the sample. The distribution of phases in the original sample is in accordance with **Table 3**. This suggests that the sample contains enough Li to form $LiAlO_2$ from all Al. The highest possible internal consumption of the available graphite in the sample is estimated to 51 %. Likely, only Al and graphite participate in the reduction CO_2 is probably not formed as a product of the reduction reaction. High content of graphite present after the thermal treatment has been seen to cause melt-in problems during pyrometallurgical processing.

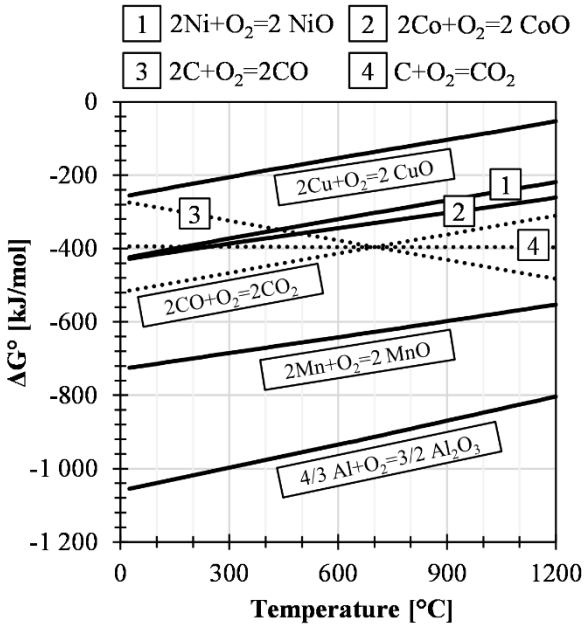

Figure 1 Ellingham diagram with oxides of interest for the current system. Calculated using FactSage 8.0.

Table 5 illustrates a summary of the events occurring in the sample during thermal treatment deduced from characterization results, thermal behavior and thermodynamic consideration. The sample after treatment at 1200°C in air was not subjected to chemical nor mineralogical characterization due to agglomeration and subsequent challenges in retrieving a representative sample. Nonetheless, considering the content of graphite in the sample treated at 720°C, and the low difference in mass loss between samples at 720 and 1200°C in air, the graphite can be assumed to still be present.

Table 5 Summary of progression in mineralogical composition upon thermal treatment.

Atmosphere→	**N.A.**	**Air**			**Inert**			
Temp. [°C] →	**Original**	**400**	**530**	**720**	**420**	**670**	**790**	**1200**
Cu	X	X	X	X	X	X	X	
Cu,Ni,Co,Mn (ss)								X
CuO		X	X					
Al	X	X	X	x	X	X	X	
$LiAlO_2$				?		X	X	X
$LiNi_{0.33}Mn_{0.33}Co_{0.33}O_2$	X	X	?		X			
Ni						X	X	
(Co,Ni,Mn)O (ss)				X		X	X	
LiF			x	X		X	X	X
C	X	X	X	X	X	X	X	X
SiO_2	X	X	X		X			

2.1.3.4 Effect of Thermal Treatment on Physical Properties

In addition to imposing changes in the chemical and mineralogical composition, the thermal treatment affects the physical properties. In air atmosphere, each consecutive increase in temperature generates a finer particle size distribution. The most significant relative changes occur between the original BM and 400°C as well as 720 and 1200°C. The former can be attributed to the partial combustion of plastic material as well as the dissociation of the binder. Based on this aforementioned sample, the difference in particle size distribution may be attributed to the continuation of combustion of the organic C. The BM thermally treated in inert atmosphere shows a similar trend as the above. However, the sample treated at 670°C was slightly finer than the one treated at 790°C. The effect the thermal treatment also results in higher density, which can be attributed to the combustion/pyrolysis of the plastic components.

Further densification is consistent with increased metallization and continuing consumption of the organic carbonaceous components.

The samples, besides the original BM, selected for fractionate analyses were based on the densification the samples treated at 720°C in air atmosphere as well as 670°C and 1200°C in inert atmosphere. The four fractions analyzed were >425, 100-425, 38-100, and <38 µm. The results will indicate which unit operation that may concentrate the transition metals or remove graphite and F.

The appearances of the four fractions of the selected samples are shown in the photographs presented in **Figure 2**. The two fractions finer than 100 µm show no visual differences between the samples. In the two coarsest fractions, i.e., 100-425 and >425 µm, of the original sample, bits of plastic can be observed. After treatment in inert atmosphere at 670°C, surfaces of metallic Cu are observed, which suggests pyrolysis of plastics without oxidation of Cu. These exposed surfaces of Cu were neither observed after combustion in air at 720°C nor after pyrolysis at 1200°C. However, based on the summary presented in **Table 5**, possible reactions with Cu were limited to surface effects.

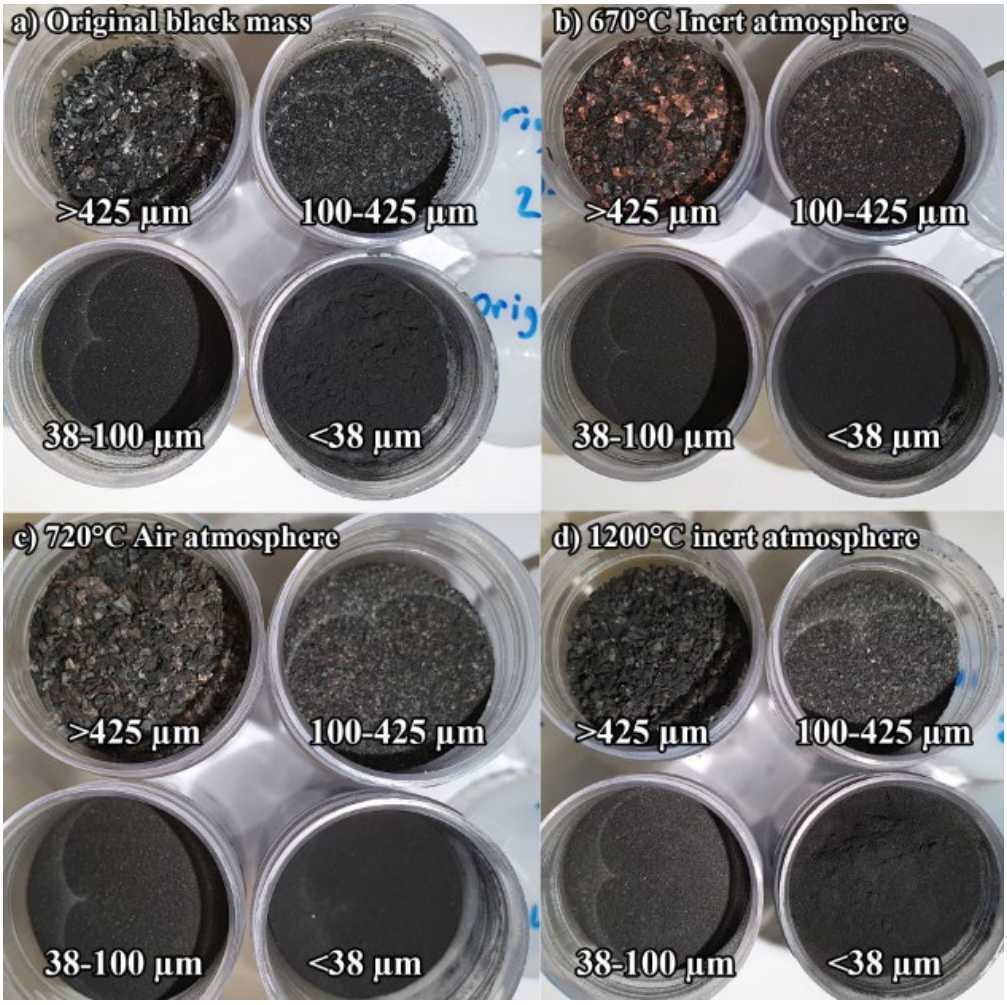

Figure 2 Photographs of the fractions of the **a)** original BM and BM thermally treated at **b)** 670°C in inert atmosphere, **c)** 720°C in air atmosphere, and **d)** 1200°C in inert atmosphere.

The major densification occurs in the coarsest fraction, which is consistent with observations of burning and pyrolysis of the plastic material. The density of the >425 µm fraction consistently increases with elevated temperatures, up to a point where possible agglomeration of, e.g., Al-containing phases may cause lower densities. A sharp increase in density observed for thermal treatments at 400 and 420°C for fractions 100-425 and 38-100 µm but much less effect in the <38 µm fraction indicate that the presence

of plastic is lower in the finer fractions. A comparatively lower increase in the fraction upon thermal treatment at 1200°C suggests high content of unreacted graphite.

The elemental distribution between the four different fractions for the original sample and the three selected thermally treated samples shows that Cu could be selectively removed from the coarsest fraction prior to the thermal treatment. However, thermal treatment at either 670°C in inert atmosphere or 720°C in air atmosphere would allow for a more selective removal of Cu since the distribution of Co, Mn, Ni, and Li in the coarsest fraction decreased upon the thermal treatment. In addition, thermally treating prior to the separation of Cu would reduce F in the Cu-rich phase. Separation of Cu prior to, or after, thermal treatment could be achieved using gravimetric unit operations.

XRD was employed to produce an indication of the distribution of graphite and suggests that the two finest fraction carries the majority of the graphite. In the thermally treated samples, these fractions also carry the majority of the Co, Mn, and Ni. Therefore, separating this fraction gravimetrically to recover graphite in an individual fraction of the BM is not feasible. As such, if graphite is not utilized effectively as a reducing agent or fuel in the thermal treatment, it has to be removed by surface-specific unit operations such as flotation.

2.1.4 Summary of WP1

In the WP1, BM composed of both cathode and anode materials, generated by treating NMC 1:1:1 battery cells, was studied aiming to identify means to remove graphite and F from the transition metals and Li. By studying the effect of thermal treatment on the BM, the following was concluded:

- Neither graphite nor F is easily removed by thermal treatment of BM consisting of both cathode and anode materials in a stagnant bed in inert or air atmosphere at temperatures ranging from 400-1200°C.
- Thermal treatment poses combustion or pyrolysis of plastics at temperatures of 400 and 420°C, respectively.
- Successively higher temperatures cause densification of the BM due to continuous combustion/pyrolysis of plastics together with an increased degree of metallization of transition metals.
- At 1200°C, Cu, Ni, and Co form liquid droplets, which upon cooling solidify as a complete solid solution.

Furthermore, the study aimed to identify possible means for separating graphite and F, gravimetrically, from the transition metals and Li after thermal treatment. Based on the results, the following was concluded:

- Cu was mainly distributed in the coarsest fraction (>425 µm) after thermal treatment at 670°C in inert and 720°C in air atmosphere, a fraction which was proposed to be removed by gravimetrical unit operations as the fraction was also the densest.
- Co, Ni, Mn, and Li were mainly distributed in the two finest fractions together with graphite and F, which, due to the physical properties, were deemed to require surface-specific unit operations such as flotation for separation.

2.2 WP2 Mapping of Li capacity in slag, and evaporation of Li from slag as function of slag composition, temperature and gas stirring (AP2: Kartläggning av Li-kapacitet i slagg och Li-förångning från slagg som funktion av slaggsammansättning, temperatur och gasomrörning).

2.2.1 Material and methods

2.2.1.1 Trial Plan

Initially, slag components of interest to vary were defined to be MnO, Al_2O_3 F and the basicity B2, whereas the content of Li was decided to keep constant, see **Table 6**. The desired slag compositions were achieved by varied addition MnO, Al_2O_3, $CaCO_3$, SiO_2, Li_2CO_3 and LiF. The chemical used in as in input materials were Li_2CO_3 (99 %, Alfa Aesar), MnO (99 %, Sigma-Aldrich), Al_2O_3 (99.9 %, Alfa Aesar), LiF (98.5 %, Chempur), $CaCO_3$ (99.5 %, Alfa Aesar), and SiO_2 (99.5 %, Alfa Aesar).

The melting temperatures of slags were predicted by the thermodynamics software FactSage FactPS-FACT pure substances database and FACT oxide database - containing data for all pure oxides and oxide solutions (solid and liquid) formed for this type of slag[12]. The temperature of 1450 and 1500°C was set as a temperature for running the experiments in the Tamman furnace and vertical tube furnace (VTF) respectively and selected as a temperature high enough for smelting the slags. It was decided to focus on four parameters that can describe the reaction systems linked to the chemistries of LCO (Lithium Cobalt Oxide) and NMC (Nickel, Manganese and Cobalt oxide) and therefore MnO was either not added or added at relatively high concentration.

Table 6 Parameters and their settings used in the design of experiments (DOE) for Tamman furnace and VTF tests.

Parameter	Parameter Type		Low level	Centrepoint	High level
Li	Constant	Quantitative	6.5	6.5	6.5
MnO	Variable	Quantitative	0	8	16
Al_2O_3	Variable	Quantitative	3	9	15
F	Variable	Quantitative	0	6.5	13
Basicity (B_2)	Variable	Quantitative	1	1.2	1.4

Table 7 Experimental plan for smelting tests in the Tamman furnace and in the VTF, compositions given in weight%.

Exp. No.	Exp. Name	Run order	Li	MnO	Al_2O_3	B2	F	LiF
7	N7	1	6.5	0	15	1.0	13.0	17.7
19	**N19**	**2**	**6.5**	**8**	**9**	**1.2**	**6.5**	**8.9**
6	N6	3	6.5	16	3	1.0	13.0	17.7
14	N14	4	6.5	16	3	1.4	13.0	17.7
9	N9	5	6.5	0	3	1.4	0	0
16	N16	6	6.5	16	15	1.4	13.0	17.7
11	N11	7	6.5	0	15	1.4	0	0
12	N12	8	6.5	16	15	1.4	0	0
3	N3	9	6.5	0	15	1.0	0	0
1	N1	10	6.5	0	3	1.0	0	0
10	N10	11	6.5	16	3	1.4	0	0
17	**N17**	**12**	**6.5**	**8**	**9**	**1.2**	**6.5**	**8.9**
4	N4	13	6.5	16	15	1.0	0	0
15	N15	14	6.5	0	15	1.4	13.0	17.7
5	N5	15	6.5	0	3	1.0	13.0	17.7
2	N2	16	6.5	16	3	1.0	0	0
18	**N18**	**17**	**6.5**	**8**	**9**	**1.2**	**6.5**	**8.9**
8	N8	18	6.5	16	15	1.0	13.0	17.7
13	N13	19	6.5	0	3	1.4	13.0	17.7

The software MODDE was used for the experimental design, it was fed with the parameters and settings shown in **Table 6,** output was the experimental plan shown in **Table 7.** As seen the Li content is kept constant whereas the contents of MnO, Al_2O_3 and F as well as the basicity B2 are varied. Li is supplied via LiF and Li_2CO_3 addition aiming to keep constant content of Li and to be being able to adjust the F content to desired value. The experiments N17-N19 (in bold text in the table) correspond to a repetition of the conditions corresponding to central point, or the middle point for each data, three times. The similar trial plan was used for tests conducted in a Tamman furnace and in a VTF but as the sample weight were roughly 150 and 20 grams, respectively, the weight of each substance differed.

2.2.1.2 Experimental procedure in the Tamman Furnace

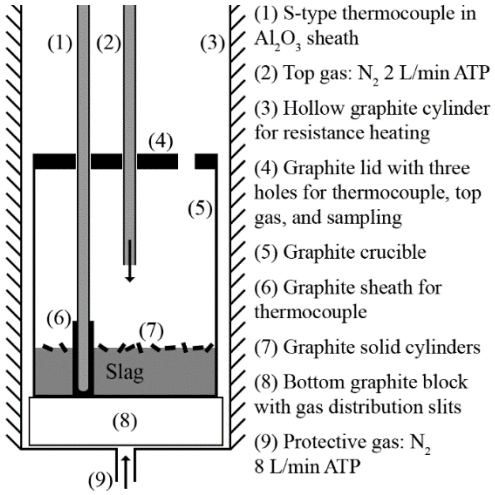

Figure 3 Test set-up in the Tamman furnace for experiments defined in **Table 7**

As mentioned, the temperature of 1450 °C was selected as a temperature high enough for smelting all slag compositions. **Figure 3** shows the crucible with the thermocouple going through the lid to the left and the alumina tube passing N_2 gas at a rate of 2 l/min (STP) in the centre. In addition to the N_2 added by the top-blowing, N_2 to shield the furnace was added in 8 l/min (STP) through the bottom, below the crucible. The rightmost hole of **Figure 3** is the sampling point where slag samples were taken using a Cu rod. The first slag sample was taken when the slag reached the desired experimental temperature. A total of seven samples were taken for each experiment, one after the temperature was reached and then after 5, 10, 20, 40, 80 and 120 minutes. Before performing the test according to **Table 7,** pre-tests of the slags without Li and F were done to select a crucible of most suitable materials. Among crucibles made of silicon carbide (SiC), magnesia (MgO) and graphite SiC was found to be least consumed during the trials. It was also confirmed that the pre-melting of slag is not needed.

For the statistically planned tests CaO, SiO_2, Al_2O_3, MnO, Li_2CO_3 and LiF were weighed to achieve the blends as specified in **Table 7** and carful mixing done before the blend were placed in the silicon carbide crucible and placed in the Tamman furnace as shown in **Figure 3**. To measure the temperature in the slag the thermocouple with surrounding alumina tube enclosed by graphite was placed in the slag.

For initial tests all sub-samples were analysed for chemical composition with focus on Li content as well as content of F. Base on initial results a selection of samples was analysed in remaining tests. Samples for chemical analyses were digested in aqua regia at 100°C, before analyses using ICP-OES. F content was analysed by ion selective electrode. Before F analyses the solid samples were fused in sodium peroxide and the fused sample dissolved in water before adding TISAB to eliminate disturbances from trivalent cations.

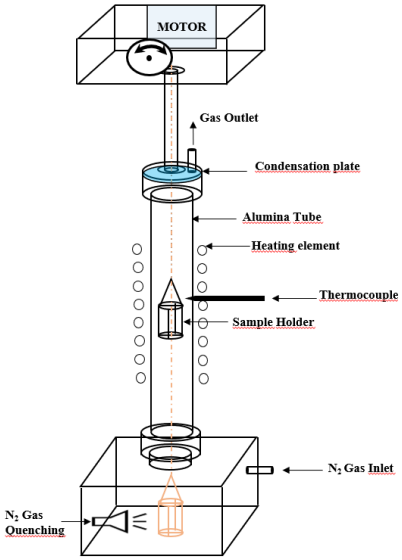

Figure 4: Schematic diagram of the vertical tube furnace.

2.2.1.3 Experimental procedure in the VTF

The 20 g samples used in the VTF tests were prepared for the statistically planned tests by mixing CaO, SiO_2, Al_2O_3, MnO, Li_2CO_3 and LiF in proportions as specified in **Table 7**. Acetone (100.0%, VWR Chemicals) was used to paste each mixture, which was then compressed at 44.48 kN to form mechanically stable briquette, and then dried for two hours at 50°C in a drying oven (Memmert GmbH).

The VTF, see **Figure 4**, used in these experiments to melt the synthetic slag was heated at 3°C/min. The holding time for each sample was set to one hour at an 1500°C using N_2(g) flow of 2 L/min. The briquetted samples were placed in a magnesia crucible and introduced into the VTF by first lowering them to the preheating zone of 800°C and held for 15 minutes to avoid foaming due to rapid melting and then to the heating zone at 1500°C for one hour. The experimental mass loss was stated by weighing each sample before and after heating. After smelting each crucible are inspected to verify successful smelting of the slag.

2.2.2 Results of melting tests in WP2

2.2.2.1 Evaluated results from the trials in the Tamman furnace and VTF.

Out of five samples with more than 20% of the Li directed to the dust four of these has an initial Al_2O_3 content of 15%. The three samples with the largest ratio of Li evaporation all initially contains 15% of Al_2O_3 and has the basicity B2=1.4. A major or large part, 50.3-90.5% of the F is directed to the dust.

In the VTF tests conducted in MgO crucible it is indicated that the presence of 16% MnO contribute to a higher yield of Li to the dust, in four out of five samples with more than 20% of Li being directed to the dust. It also seems more likely to get a higher evaporation of Li at higher slag basicity in the VTF tests. The remaining amount of slag after VTF tests, after subtracting the MgO, is in most samples higher than the amounts estimated by thermodynamic modelling in Factsage for the corresponding samples. The replicates 18 and 19 are quite similar in chemical composition and slag amount, but sample 17 differs significantly and must be considered as an outlier.

2.2.2.2 Thermodynamic calculations to explore the VTF test results

Results for slag and gas phase from thermodynamic calculations up for every 50 °C up to 1500°C. The ratio of introduced Li and F directed to the dust is in general lower in the experiments than theoretically estimated, for F the deviation is less in the Tamman furnace tests. The evaporation of Li is slightly higher in the VTF tests, but it is significantly lower that estimated in thermodynamic calculations.

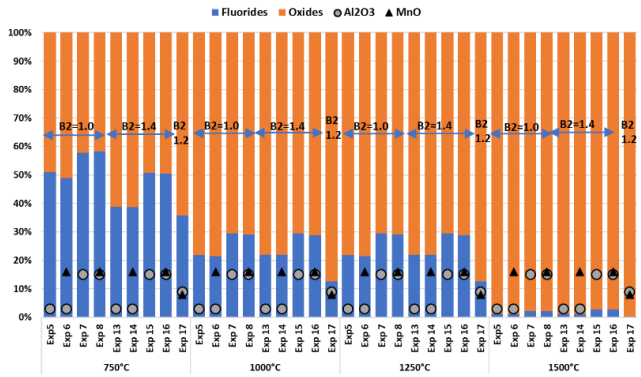

Figure 5 Share of fluorides and oxides in the slag at 750, 1000, 1250 and 1500°C, B2 and added MnO and Al_2O_3 are indicated. 6.5% of F is assumed to be added in Exp. 17, 13% of F in all other experiments.

According to thermodynamic calculations the fluorides in the slag contribute to molten metal fluorides, dominating the slag at 750°C, **Figure 5**. Assuming a temperature of 1500°C, thermodynamically, the slag is dominated by oxides. Thermodynamic calculation results for 1500°C is showed as an example. Components present at lower amounts than 0.001 grams are excluded. At 1500°C the amount of LiF directed to the gas is high and the slag is dominated by oxides, see **Figure 6** and **Figure 7**. It is estimated that in these samples with 15% of Al_2O_3 present in the initial slag, 2.4 and 2.5 g of $LiAlO_2$ are still solid at 1500°C in Exp. 15 and Exp. 16. Added MnO is predicted to be present in the slag mainly in the form of Mn_2O_3 at 1500°C. With the addition of MnO the dissolution of MgO from the crucible is less, especially for the experiments with basicity of B2=1.0. The presence of F in the samples enhances the dissolution of MgO into the slag and MgF_2 is formed, the effect is greater at lower B2.

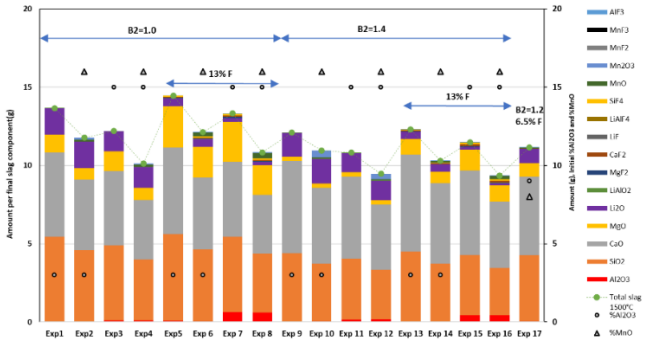

Figure 6 Initially added slag components, single basicity and thermodynamically estimated slag amount and composition at 1500°C.

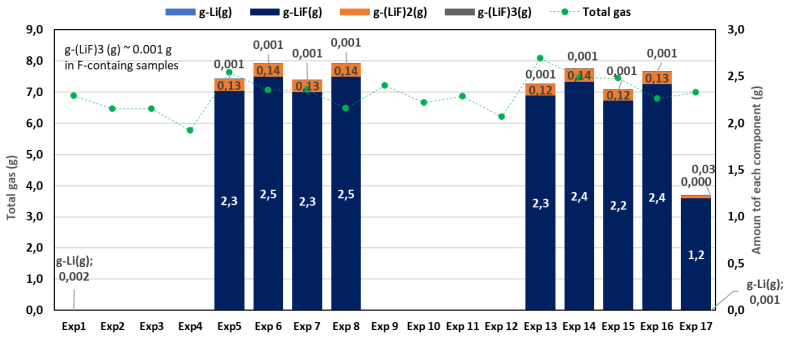

Figure 7 Gases estimated to be formed at 1500°C according to thermodynamic calculation.

2.2.3 Summarized discussion of WP2 results

The experimental results and the thermodynamic calculations indicate that the presence of F is crucial for the evaporation, thermodynamically the evaporation is estimated to be through LiF, $(LiF)_2$ and $(LiF)_3$. Therefore, under the applied conditions it is not possible to direct Li to the dust while F remains

in the slag. In general, the results indicate a higher evaporation of LiF for F containing samples with higher initial Al_2O_3 content in the slag, in those samples solid $LiAlO_2$ is remaining at 1500°C according to the thermodynamic calculations. The slag design can be done based on other considerations than used in this study, e.g. as done in the pilot tests at Swerim.[13] In those tests the lime was added to join with Al_2O_3 forming calcium aluminate slag, this slag has significantly higher basicity. During the pilot trials up to 68% of the Li was directed to the slag [13] compared to around maximum 43% in the laboratory experiments. Further, as BM was melted in these tests Li ions could be reduced and evaporated as metallic Li, later in the off-gas channel an oxidizing atmosphere with CO_2 exists, and Li could be oxidized and form e.g. Li_2CO_3 that was the major Li compound in the dust. Evaporation of LiF present in the slag could maybe explain the presence of LiF in the dust. Besides the difference in slag properties, more turbulence in the pilot tests may contribute to overcome the kinetic limitation. The results indicate that further optimization of the slag composition can enhance the thermodynamics of evaporation, additionally, the kinetic limitations can be studied in more detail to find solutions to lower this effect.

The Li and F evaporation is less in the experiment compared to in the thermodynamic estimation, which may be due to kinetic limitation. Comparing the distribution of Li and F between the slag and dust for the Tamman furnace and VTF tests, the general trend is that the F removal is higher in the Tamman furnace tests, whereas the Li evaporation is higher in the VTF tests. Thermodynamic calculations could reveal how the use of SiC crucible influence the slag system and thereby the evaporation of Li and F, thermodynamic calculations will be conducted beyond the end of this project and be included in a planned scientific open-access publication. It is possible that additional SiF_4 is formed if the crucible material (SiC) interacts with the slag, which may influence the speciation of F.

The presence of F enhances the slag melting by the formation of fluorides with low melting point, but at higher temperatures, possibly lower F content in the slag due to the evaporation may cause solidification of part of the slag. At temperature of around 1450-1500°C the majority of the slag is melted. In the practical experiments F containing compounds in the slag may possibly contribute to lower viscosity, which is beneficial for mass transfer in the slag, by that the kinetics of LiF evaporation can be enhanced. Also, a slightly higher basicity may lower the viscosity above the melting point of the slag, and contrary, remaining solid particles may contribute to higher viscosity.

The thermodynamic calculation results shows that it is a valuable tool able to predict interaction of slag with the crucible material and give advice about adjusted slag design as well as choice of crucible. If using a MgO crucible, the crucible can be protected by the addition of MgO.

2.3 WP3 optimization of Li distribution to dust with sustained quality of metal alloy and possible recovery of slag. (AP3: Optimering av fördelning av Li till stoft med bibehållen kvalitet av metallegering och möjlig återvinning av slagg)

2.3.1 Material and methods in WP3

2.3.1.1 Sample of Black Mass

Based on the results from work package WP1, the BM thermally treated at 720°C in air was the most promising material from an industrial perspective. For BM treated under these technically simple conditions 67 % of all F was removed while all Li remained in the sample. Therefore, this sample was used in WP 3. The chemical composition of this BM is presented in **Table 8**.

Table 8 Chemical composition of BM treated at 720°C in air atmosphere.

Cu	F	C	Al_2O_3	CoO	MnO	NiO	Li_2O
10.00	1.50	13.30	8.87	8.42	9.98	12.43	9.11

2.3.1.2 Thermodynamic Calculations

Based on the preliminary results of WP 2, the slag composition presented in **Table 9** gave the most promising results in terms of Li evaporation. The results from WP 2 were preliminary in the sense that the slags containing F were not evaluated yet. Thermodynamic calculations were used to design the pyrometallurgical experiments with ingoing slag formers and BM to generate a bottom alloy, slag and dust. The thermodynamic calculations were utilized to determine if, and how much, of additional compounds that were required to consume the remaining carbon in the BM. All calculations were based on 100 g of thermally treated BM with composition according to **Table 8**. Additions of CaO, Al_2O_3, and SiO_2 were iterated to estimate required amounts to reach a slag composition similar to the one in **Table 9**, and one calculation was done to determine the amount of MgO required for saturation.

Table 9 Slag composition from WP 2.

	CaO	SiO_2	Al_2O_3	B2
Value	48.16 wt.%	34.40 wt.%	17.44 wt.%	1.40

The calculations were performed using FactSage 8.1 with databases FactPS, FToxid and FTmisc. FTmisc-CuLQ was used to describe the bottom allow as the phase is optimized together with FToxid-SLAGA, which was used to describe the slag phase. The former solution (FTmisc-Cu-LQ) does not contain a description of Co, although this element can be assumed to go into solution with Cu. Therefore, metallic Co was included in the calculations, and this was assumed to enter the Cu. FTmisc-FeLQ was included in cases where Fe_2O_3 was added to react with carbon. FactPS was used to describe pure solid phases and the gas phase. Other solution phases included were FToxid-SPINA, FToxid-MeO_A, FToxid-WOLLA, FToxid-bC2SB, FToxid-Mel_A, FToxid-OlivA and FToxid-CORU.

2.3.1.3 Vertical Tube and muffle furnace Experiments

The experiments in WP 3 were carried out in the VTF with the setup illustrated in **Figure 4**. Each experiment was carried by heating from ambient temperature to 1500°C at a heating rate of 3°C min^{-1}, a subsequent dwell time of 180 min at 1500°C and finally cooling to room temperature at a cooling rate of 3°C min^{-1}. A N_2 flow of 8 L min^{-1} was applied from ambient temperature and pressure (ATP) up to 720°C to flush the furnace and acquire an inert atmosphere. After 720°C and throughout the rest of the heating cycle, 1 $Lmin^{-1}$ ATP N_2 was added to maintain the inert atmosphere, but simultaneously generate a lower flow to support condensation of formed gases on the water-cooled condensation plate.

Table 10 Experiments performed in the vertical tube furnace.

Experiment	**Exp. 1**	**Exp. 2**	**Exp. 3**	**Exp. 4**	**Exp. 5-8***
Atmosphere	Inert	Inert	Inert	Inert	Air
Crucible	SiC	SiC	SiC	MgO	MgO
Black mass [g]	50.00	50.00	50.00	50.00	50.00
$CaCO_3$ [g]	16.87	16.49	37.82	37.82	37.82
SiO_2 [g]	6.75	6.60	15.14	15.14	15.14
Al_2O_3 [g]	0	0	4.50	4.50	4.50
Fe_2O_3 [g]	0	16.50	16.50	16.50	16.50
MgO [g]	0	0	0	4.50	4.50
Idea	Lowest possible slag amount.	Lowest possible slag amount, C consumption.	Higher slag amount to promote reduction of FeO_x in slag.	As Exp. 3 but with MgO crucible.	As Exp. 4, but in muffle furnace.

Table 10 shows the experiments performed in WP3. The first three experiments were carried out in a SiC crucible and due to interaction between the crucible and the bottom alloy the fourth experiment was carried out in an MgO crucible. To prevent interaction with the slag, MgO was added to a concentration surpassing the saturation limit. After each experiment, the crucible was removed from the furnace and the solidified molten part was collected separately from non-molten material. The dust condensed in the tubes and on the condensation-plate was collected. The tests in air atmosphere were conducted in a muffle furnace heated at 5°C/min up to 1500°C followed by a hold time of one hour before cooling

down. The dust sample was collected after the test, but due to breakage of the crucible leading to loss of the major part of the melt it was not possible to collect the remaining sample. The first test (No. 5) was conducted without sucking air through the sample container, whereas a peristaltic pump was used in the following tests. In the last two tests the alumina tube was partly plugged during the test, and less dust was collected after test 7-8 than after test 6.

The collected dusts from all lab tests as well as a sample collected at during pilot tests at Swerim were characterized for the planning of leaching experiments. The dust and non-molten material were characterized using X-ray diffraction (XRD). Selected samples of the bottom alloy and slag phase were cast in epoxy and polished according to standard metallographic methods. The samples were subsequently characterized using scanning electron microscopy together with energy dispersive X-ray spectroscopy (SEM-EDS). In addition, some samples were characterized using laser ablation connected to an inductively coupled plasma mass spectrometer (LA-ICP-MS) to analyze the Li content in specific phases.

2.3.2 Results and discussion

The experiments yielded three fractions that were analyzed separately.

- melted and coalesced referred to as the molten portion of the sample
- powdery fraction present in the crucible referred to as the non-molten part of the sample.
- dust collected from the water-cooled plate at the top of the furnace referred to as the top dust.

Table 11 presents the ingoing mass in each experiment and the weight of each outgoing fraction. For both Experiment 1 and 2, no molten fraction was present in the bottom of the crucible. Thus, the mass present in the crucible was classified as non-molten. However, in the subsequent analyses, a pair of tweezers was utilized to extract pieces of agglomerated material, which was analyzed and classified as molten. In experiment 4, and 5-8 it was not possible to collect the molten fraction due to loss of melt.

Table 11 Mass balance of each experiment.

Experiment	Ingoing [g]	Molten Fraction [g]	Non-molten Fraction [g]	Top dust [g]	Total Outgoing [g]	Difference In-Out [g]
1	73.62	/	51.63	0.45	52.08	21.54
2	89.89	/	58.11	0.96	59.07	30.82
3	123.96	66.49	12.84	0.70	80.03	43.93
4	*X*	*Y*	*Z*	*W*	*V*	*R*
5-8	*X*	*Y*	*Z*	*W*	*V*	*R*

2.3.2.1 Characterization of Molten Portion of Samples

Due to the loss of melt in the muffle furnace tests, only was sample 1-3 heated in inert atmosphere that could be evaluated by SEM-EDS. Five different phases crystallized in the slag during the cooling of the sample, none of these phases hold the transition metals, which suggests that the slag composition is suitable. The compositions of the five different phases suggest presence of e.g. CaF_2, CaS, $Ca_2SiFO_{3.5}$, and calcium aluminosilicate phases.

In Experiment 2, iron oxide in the form of chemical grade hematite was added to consume graphite available in the BM and all iron oxide dissolved by the slag was reduced and entered the metallic phase. The standard deviation of the EDS analyses of the metallic phase is large, suggesting that two metal phases may be formed. Five different phases defined showed that all transition metals in the molten sample are reported to the metallic phase, which indicate that the graphite could be consumed, and the melt-in behavior is favorable. However, the melt-in behavior of the present setup was not ideal as a large portion is not molten. The EDS analyses suggested that the stoichiometries of the crystallized phases were $Ca_2SiFO_{3.5}$, CaS and two different calcium aluminosilicates.

In Experiment 3 is presented in the wire suspending the crucible broke during the dwell time at the

highest temperature and, therefore, the sample was rapidly cooled in the quench box. Consequently, the slag was not allowed to form several phases. Instead, two distinct phases were identified for which the analysis indicate $Ca_2SiFO_{3.5}$ and a type of calcium aluminosilicate. In addition to analyzing spots of the individual phases, zones representing both phases were analyzed with the EDS, which suggested an overall slag composition as presented. All iron oxide in the slag phase was reduced in the experiment and none of the transition metals present in the BM reported to the slag phase.

Table 12 Average EDS analyses [at.%]) related to slag area in sample from Experiment 3.

	Ave.	Std.dev.
O	56.1	1.0
F	6.4	0.6
Al	7.9	0.6
Si	11.3	0.4
S	0.2	0.0
Ca	18.0	0.6
Mn	0.1	0.1

Figure 8 presents a photograph of the molten portion of the sample together with the crucible, taken after Experiment 3. In the bottom of the outside of the crucible, metallic droplets can be seen. This indicates that formed iron consumed the SiC crucible and based on this observation MgO crucibles were used in the subsequent experiment.

Figure 8 Photo of the molten part of the sample (left) and the crucible (right) after Experiment 3.

The analysis results follow the quality assurance quality control (QA/QC) protocol showing that all elements except iron were analyzed accurately, the analyses tend to overestimate the iron content. Challenges were faced during the analyses as crystallized phases were not forming large grains suitable for ablations and the inhomogeneity of the rapidly cooled sample from Experiment 3. By using 100x100 µm spot sizes, the inhomogeneity challenge was addressed well. The most accurate data on the Li content in the slag phase was generated for Experiment 3, suggesting that 2.8 wt.% was present in the slag, which is consistent for Experiment 2 as well, i.e., the slag phase had a lower mass, which resulted in a higher concentration of the available Li. The transition metals were not detected to high extents in the slag phase. The somewhat high concentration of 19 ppm Cu in the slag of Experiment 3 was attributed to partial ablation of metallic phases in 20% of ablations.

2.3.2.2 Characterization of Non-molten Portion of Sample

The non-molten portion of the samples was analyzed using XRD and the main phase in the non-molten portion after Experiment 1 was graphite, which is reasonable considering that nothing was added to consume carbon. In addition to graphite, the non-molten fraction contained phases that resemble the slag phases identified in the SEM-EDS analyses, e.g., $Ca_2SiFO_{3.5}$, $Ca_2Al_2SiO_{3.5}$ and CaF_2. Furthermore, wide peaks of Cu were identified, which is consistent with the solid solution of Cu-Mn-Ni-Co formed in the experiment. The only phase, except graphite, original to the BM was $LiAlO_2$.

In Experiment 2, iron oxide was added to consume the graphite and aid in the formation of a separate metal and slag phase. Iron oxide was not detected in the slag phase, and the amount of iron oxide added corresponded to complete consumption of graphite. Thus, the remaining graphite suggests that the SiC crucible participated in the reduction as well. The results are consistent with those of Experiment 1, i.e., the non-molten fraction is, in fact, molten but not coalesced into a continuous phase.

In Experiment 3, hematite was added prior to the experiment. However, the amount of slag was significantly increased. The aim was to improve the wetting of graphite and thereby the reduction of dissolved iron oxide present in the slag. The approach appeared superfluous as the non-molten portion of Experiment 2 was completely reduced. The results in Experiment 3 are consistent with Experiment 1 and 2. Since the wire suspending the sample in Experiment 3 broke, additional information can be retrieved as the slag had less time to crystallize, and both the non-molten and molten portion of the sample showed the similar two oxidic phases. This strengthens the conclusion that graphite hinders the coalescence of the slag and metallic phase rather than hindering the actual melting.

2.3.2.3 Characterization of the collected dust

The dust collected from the water-cooled plate in the top of the VTF and in the glass flask and tube after the muffle furnace was characterized using XRD. The concentration of several of the components is higher in dust from experiments 7-8 compared to in dust from experiment 5, one reason could be that problems with plugging resulting in less air passing and thereby conditions with lower oxygen availability is created. This is also indicated by significant peaks for LiF. Some carbonate diluting the sample may have been formed in experiment 5.

Table 13 Chemical composition of two dusts samples collected after tests in the muffle furnace.

	Al	Co	Cu	Li	Mn	Ni	S	Si	Na	Ca	Ca	K	Mg	F
Dust test 7-8	0.243	0.0110	0.0589	19.8	0.162	0.261	13.9	27.2	10.3	10.9	0.967	10.43	0.495	26,4
Dust test 5	0.262	0.0056	0.0320	3.02	0.0357	0.0535	0.263	20.0	0.334	0.806	0.824	0.164	0.200	3.60

Comparing the Li compound reference patterns with the diffractograms of the dusts shows formation of LiF in all experiments. Furthermore, based on the relative intensity of LiF in the samples, the XRD analyses suggest that LiF is the dominating phase in all dust samples formed during VTF tests in inert atmosphere. The only Li phases, apart from LiF, that are possible in the samples are Li_2CO_3 in Experiment 2 and 3 as well as Li_2O in Experiment 3. The latter is less likely based on the diffractograms. Of the dust formed during muffle furnace tests in air, the first test conducted in air is indicated to contain mainly lithium fluoride (LiF), in the test without pump presence of silicate was indicated as well. In the tests with a pump connected the peaks corresponding to LiF are more prominent.

2.3.2.4 Characterization of the collected dust from pilot tests in EAF

The dust samples from the pilot tests were characterized in more detail, and both XRD and chemical composition of the sample suggests presence of LiF and Li_2CO_3 and possibly some Li_2O. Li_2CO_3 dominates in this dust sample, which can be expected due to the conditions in the off-gas channel of the EAF, the more oxidizing conditions and with CO_2 present. According to the diffractograms, non-Li-containing phases are present as well. KCl and NaCl were suggested phases in the dust from Experiment 2 and 3. Also, several hydrocarbons were suggested to explain the observed peaks. However, based on the one-dimensional characteristics of XRD and the scarce information about the sample, conclusions on additional phases were deemed non-accurate. However, if judging from the chemical composition of dust collected after muffle furnace other compounds seems possible.

2.3.3 Summary of WP 3

The smelting tests in WP3 was conducted using the most promising slag composition for Li evaporation and based on the results from WP1, the BM thermally treated at 720°C in air was used in the tests. Interaction with the SiC crucible made it necessary to change to MgO crucible, but then the slag had to be saturated with MgO to avoid dissolution of the crucible material. The optimum test design for

producing dust was identified and dust characterized. It was not possible to produce enough of dust for leaching tests, instead the dust produced on pilot scale during BM smelting in EAF received from Swerim was used in the leaching experiments in WP4.

Based on the results, the transition metals report to the metallic phase, which shows that the chosen slag composition will not negatively affect the possibility of recycling the valuable metals in the BM. Furthermore, the characterization of the top dust collected at the water-cooled plate shows that Li evaporates, which suggests that hydrometallurgical methods can be employed to recover Li from the dust. However, although the slag composition was designed to maximize the evaporation of Li, the LA-ICP-MS analyses suggested that Li is still present in the slag in significant concentrations after the experiments.

The Li phases present in the dust are influenced by the atmosphere. At higher oxygen potential EAF dust and dust produced in the laboratory experiments contains mainly Li_2CO_3 and under inert conditions LiF dominates. The Li_2CO_3 may be formed when evaporated metallic Li react with the off gas containing CO_2 and having high oxygen potential.

2.4 WP4 Process improvement for dissolution and extraction of Li in dust formed in the melting process. (AP4: Processförbättring för upplösning och extraktion av Li från lösning för återvinning av Li från stoftet bildat vid smältprocessen)

2.4.1 Materials and methods

2.4.1.1 Flue Dust Characterization

The dust produced during treatment of BM in an EAF[13] was divided into equal subsamples for which chemical elemental composition was determined by ICP-OES (Model: Thermo Scientific ICAP 7200 DUO, Thermo Fisher Scientific, Waltham, MA, USA). For the analysis of F content, fluoride ion selective electrode method similar as in WP1 was used.

The existing phases and their distribution were analyzed by a PANalytical Empyrean X-ray diffractometer (XRD) equipped with Cu Kα radiation of 45 KV and 40 mA and a Zeiss Gemini Merlin Scanning Electron Microscopy coupled with Energy dispersive Spectroscope (SEM – EDS). For SEM, the analysis was conducted on a thin layer of powdered specimen which was applied onto adhesive carbon tape. The acceleration voltage was set to 3 kV and the emission current was 8 pA.

The chemical composition of the dust is stated in **Table 14,** the XRD analysis indicated the presence of Li mainly as Li_2CO_3 but also LiF and Li_2O. All concentration of the other elements shown in **Table 14** may become part of the leachate and can potentially give impurities in the recovered Li product. The size fraction analysis of flue dust by SEM imaging presented in **Figure 9** depicts that most of the flue dust was in the size range 0.5 to 1 μm, however, some of the particles were also up to 3 μm.

Table 14 Elemental composition of the EAF dust produced during tests at Swerim [13]

	Li	Co	Mg	Ca	Na	K	Si	Al	Mn	Ni	Fe	S	Cr	Zn	F
Wt.%	14.1	0.29	1.02	2.50	0.64	0.67	0.94	1.46	4.56	2.95	1.94	0.45	0.10	1.82	5.29

2.4.1.2 Leaching methods

Leaching methods was selected based on the previous pre-study on synthetic material[14] and the properties of characterized Li-rich dust. Leaching was conducted with carbonated water, lime water, and carbonated water with lime water addition in 150 ml ultrapure water for 2 hours at a constant stirring rate of 300 rpm under varying S/L ratios (0.05 – 0.1 g/ml) and at temperatures of 24, 50 and 75°C. The temperature and stirring rate were controlled by Velp Scientifica AREX – 6 hot plate stirrer system

coupled with VTF digital thermoregulator. The CO_2 gas flow rate and Ca/Li ratio for the respective system was maintained at 0.5 L/min and 1.2, respectively. When combining carbonated water and lime water, $Ca(OH)_2$ was added stoichiometrically corresponding to the LiF content in the flue dust. In all experiments, pH was measured using a Metrohm 6.0259.100 connected to a ThermoScientific Orion Star A221 pH meter, while the redox potential was measured using a Metrohm 6.0451.100 connected to a ThermoElectron Orion 3-Star pH meter. Samples were then collected at leaching time of 5, 10, 20, 60 and 120 mins and filtered through a 0.45 µm nylon syringe filter before preservation in 2 % nitric acid for ICP and fluorine analysis as described in 2.4.2.1. At the end of each experiment, the leaching solution was filtered, and the leach residue dried and preserved for further analysis.

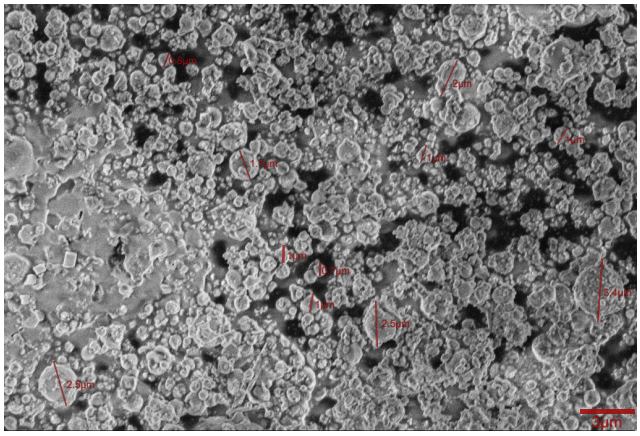

Figure 9 SEM image of the EAF dust produced in pilot scale test.

2.4.2 Results and discussion of WP4

For the leaching 0.05 to 0.1 g/ml flue dust in carbonated water, the dissolution rate at both S/L ratios slowed down just after the first 5 mins and appeared to reach equilibrium after 60 mins of leaching time. At S/L ratio of 0.05 g /mL, the final dissolution of Li was roughly 70% at 25 and 50°C. Increasing the S/L ratio from 0.5 to 0.1 g/mL resulted in lower final Li dissolution and an increase in temperature impacted the final Li dissolution negatively. Higher S/L ratios can introduce a restriction to mass transfer of the liquid to the solid surface, possibly leading to incomplete dissolution of Li_2CO_3. For dissolution of 0.05 to 0.1 g/ml flue dust under lime water, the rate of dissolution for both S/L ratios was very fast in the beginning and reaction seem to reach a plateau with the first 10 mins of leaching time. The temperature had a positive impact on the rate of dissolution and final dissolution of Li that reached up to 77%. The results were slightly lower at 0.1 g/ml. Finally, for flue dust under carbonated water and lime water, the leaching behaviour was quite similar as for flue dust leaching with carbonated water.

The flue dust contains around 65.2 % of Li_2CO_3 and 7.22 % of LiF. According to the experimental yields achieved for synthetic materials in the previous study[14], the final possible Li dissolution for flue dust in carbonated and lime water was estimated to 82% and 89 % respectively. However, the final dissolution for the flue dust came out to be 70 % and 77 %. This lower dissolution efficiency for the actual dust may be due to passivation of the surface of Li bearing particles. The flue dust contains 6.58 % Mg as MgO and 2.5 % Ca as CaO (**Table 14**). In case of carbonated water leaching, the oxides of Mg and Ca may have reacted to form carbonates forming a passivation layer on the surface of Li_2CO_3, inhibiting further dissolution. The XRD analysis of leach residues depicts the $CaCO_3$ along with undissolved LiF and Li_2CO_3. The SEM analysis of carbonated water leaching of flue dust also indicate the presence of a passivating layer which might have hindered complete dissolution of Li resulting in lower-than-expected final Li dissolution.

For lime water leaching of flue dust, Li_2CO_3, LiF, $CaCO_3$, $Ca(OH)_2$, and CaF_2 are detected in the residue. Notably, LiF is not detected at 75°C, indicating that its concentration could be below the detection limit

of XRD. These results and the SEM analysis indicates possible presence of $CaCO_3$ and CaF_2 on the surface of Li-bearing minerals.

Leaching with a combination of lime and carbonated water resulted in a residue quite similar to that of carbonated water leaching. The SEM images of the leaching residues also in this case indicate possible surface passivation of Li bearing species i.e., by the precipitated $CaCO_3$ and CaF_2. The XRD diffractogram shows undissolved Li_2CO_3 and LiF along with $CaCO_3$ in the leach residue. Incomplete dissolution of Li_2CO_3 might be due $CaCO_3$ passivating the particle surfaces, which was indicated by SEM analysis and SEM images.

The recovery of Li through crystallization and the possibility to reach sufficient purity of formed Li hydroxide was studied through antisolvent crystallization. The lime leaching of flue dust resulted in a Li dissolution of 77 % but also with different impurities was co-leached. The concentration of pregnant leaching solution (PLS) obtained during lime leaching along with the allowable limit of co-dissolved impurities in commercial lithium hydroxide monohydrate ($LiOH{\cdot}H_2O$) as a battery precursor is presented in Table 15. The allowable limits were adapted from [15]. Apart from Cu, the concentration of all the co – leached impurities exceed the allowable limit significantly, necessitating their removal to achieve battery grade $LiOH{\cdot}H_2O$.

Table 15 Concentration of co-leached impurities for flue dust in lime water (S/L ratio 0.05 g/ml, nCa/nLi =1.2, 75 ˚C) in comparison to allowable impurity limit in commercial $LiOH{\cdot}H_2O$

Element	Li	Na	K	Ca	Cu	Al	Zn	S	Cr	
PLS	5567	290.68	276.51	81.05	3.20	78.56	98.87	189.31	74.33	ppm
Allowed	N/A	20	10	15	5	10	10	≤ 4000	5	ppm

Crystallization emerges as a viable recovery process when the concentration of targeted metal ion is relatively high. Therefore, to recover high purity $LiOH{\cdot}H_2O$ from the PLS antisolvent crystallization was applied. The technique involves addition of water miscible organic solvent to reduce the solubility of solute which generates supersaturation and targeted salts are crystallized [16]. Critical steps for anti-solvent crystallization are the selection of appropriate right antisolvent(s), screening tests to determine the effectiveness of antisolvent and optimisation of organic to aqueous phase ratio.

Table 16 Specifications of selected antisolvents for $LiOH{\cdot}H_2O$ crystallization [17]-[19]

Antisolvent	Molecular mass, g/mol	Density, g/ml	Boiling point,°C	Dielectric constant	Viscosity, cP	Water Miscibility	LiOH solubility, 20°C
Ethanol	46	0.789	78	24.5	1.1	Highly miscible	2.36 g/100 g
Acetone	58	0.784	56	20.7	0.36	Highly miscible	insoluble
Isopropanol	60	0.803	97	20,1	2.256	Highly miscible	Insoluble
Ethylene glycol	62	1.11	197	37	18.4	Highly miscible	Insoluble
Ethyl Acetate	88.11	0.902	77.1	6.40	0.443	Highly miscible	insoluble

The choice of antisolvent is critical for achieving a good recovery of the targeted salt. Typically, the main aspects considered for appropriate solvent selection are [17] a solvent with lower dielectric constant than water, as it decreases the solvation of charged ions and the solubility of solute is reduced. For efficient filtration and washing low viscosity liquids are preferred. The boiling point and heat of vaporisation are important for the separation and generation of antisolvent. Additionally, is should not be reactive with aqueous phase components and electrochemically inert. Based on these aspects 5 antisolvents namely methanol, ethanol, isopropanol, acetone, ethylene glycol and ethyl acetate were selected for screening tests. The properties of these 5 antisolvents are presented in **Table 16**.

The primary goal of tests is to identify antisolvents which can crystallize $LiOH{\cdot}H_2O$ from the PLS and then optimize the crystallization parameters in up-coming studies beyond the project end. The screening

tests conducted in an incubator shaker to keep the temperature constant, and achieve proper mixing. Each of the five antisolvents were mixed with the PLS at O/A volumetric ratios of 3 and 6 mixed during 72 hours and at 25°C. For the screening tests, 20 ml of PLS was mixed all at once with the respective organic liquid to have the A/O ratio of 3 and 6. After completion of tests, the mixture was filtered, and the filtered solution was sampled for analysis by ICP-OES. The results of screening tests depict that ethanol and ethylene glycol performed poorly in terms of Li crystallization, ethyl acetate was not selective, and it has the lowest di-electric constant of 6.40. Acetone and isopropanol resulted in a high crystallization yield for Li, with less co-crystallization of impurities. Therefore, these two antisolvents were selected for further investigation and optimization. Following the selection of proper antisolvents, experiments were then conducted to determine the proper O/A ratio for high recovery of Li but with minimum recovery of impurities. For this the solvents (acetone and isopropanol) were mixed with the PLS in the O/A volumetric ratios of 0.2:1, 0.5:1, 1:1, 2:1, 4.1 and 5:1. Like in the screening tests, acetone and isopropanol were added all at once to the PLS and the temperature and agitation rate were constant at 25°C and 150 rpm. For both antisolvents, it was observed that with increasing O/A ratio, the crystallization of Li increased and reached a maximum of 96 % and 76 % for acetone and isopropanol respectively at O/A of 5. However, the co-crystallization of impurities also increased with increasing O/A ratio. The optimal O/A ratio for Li crystallization was identified as 4 for acetone and 5 for iso propanol.

Summarized results of WP 4

Of the Li contained in BM melted in the EAF about 68.3% and 60.9% of the Li was directed to the dust[13], characterization of dust showed that the Li was distributed between to major compounds present at around 65.2 % of Li_2CO_3 and 7.22 % of LiF. The highest leaching recovery for leaching of flue dust in carbonated and lime water achieved was 70 % and 77 %, respectively. Estimation of possible leaching efficiencies based on the dust composition and leaching efficiencies of synthetic Li_2CO_3 and LiF in the previous study [9] was 82% and 89 %, respectively. The lower dissolution efficiency for the actual dust indicates a potential inhibition of the dissolution that also was indicated by the SEM evaluation of leach residue.

The optimal O/A ratio for Li crystallization was 4 for acetone and 5 for isopropanol, for these conditions 93% and 76% of the Li was crystallized, however, the impurity content is still too high but is believed to be possible to lower through stepwise addition of the antisolvent. In future optimization tests as well as freeze crystallisation will be conducted. Based on the findings in WP4 further studies will be conducted in continued research in other projects. Regarding crystallization these may concern the impact of crystallization time and antisolvent feeding rates on crystal growth, particle size distribution and impurity crystallization.

2.5 WP5 Techno-economical assessment of proposed process (AP5: Teknoekonomisk analys kopplat till den föreslagna processen.)

2.5.1 Studied process steps relative state-of the art and battery regulation

To align with the battery regulation [20] an overall LIBs recovery rate of 70% by 2030, and 95% recycling of Co, Cu and Ni, and 80% of Li by 2031 must be achieved. To reach an overall recovery of 70% may be difficult before regeneration of graphite is realised, as the content of graphite in LIBs may be 20-30 wt.%.

The studied process steps are included process flow sheet consists of pyrometallurgical and hydrometallurgical steps, a comparison to other methods like those in **Table 17** cannot be done in detail

as quantitative data for the processes are not available. Principle differences that are advantageous for the studied process in comparison to other processes[21] identified to be relevant are the following.

Pre-treatment and graphite recovery: In some processes the sorted batteries are directly into a smelter, this is cost effective as pre-treatment is not required recovery of e.g. graphite is not possible. In general, in the processes in **Table 17**, graphite is not recycled but consumed in the reduction of oxides in the LIBs and of additional oxides added, this will contribute to CO_2 emissions. Recovery of the major part of the graphite is necessary if an overall circularity of 70% of LIBs shall be reached.

In the present study thermal treatment of BM consisting of both cathode and anode materials of NMC 1:1:1 was conducted in a stagnant bed in inert or air atmosphere at temperatures ranging from 400-1200°C. It was not possible to remove F or separate graphite easily but two the following facts about pretreatment that can be further developed was found.

Table 17 Examples of existing combined pyro and hydro processes compared to the one evaluated in the project[21], SX=solvent extraction, RHF = rotary hearth furnace, SAF=submerged arc furnace

	Pretreatment	Pyro	Post treatment	Products	Secondary products	Losses
This Process	BM thermal treatment, physical sep.	EAF smelting	Leaching of dust	Metal alloy (Cu-Co-Ni-Mn-Fe) $LiOH*H_2O$	Slag, ~30% of Li	Plastics, electrolyte leach residue
Umicore	No	Smelting shaft furnace	Leaching, SX	$CoCl_2$, Co, Ni, Cu, Fe	Fe, Li, Mn	Electrolyte, plastics, graphite
Xstrata (Glencore)	No	Pre-conditioning in rotary kiln Smelting in EAF	Hydrometallurgy	Alloy Co-Ni-Cu	Li and Mn in slag	
Inmetco	Sorting,	Calcination (RHF) Smelting (SAF)	Iron casting	Alloy Co-Ni-Fe	Li slag	Organic material used as chemical reagent
Accurec	Sorting, dismantling, pyrolysis, milling separation, agglomeration, filtration	Smelting	Acid leaching	Co-alloy Li_2CO_3	Metallic alloy	Electrolyte, polymer, graphite
JX Nippon Mining and Metals	Incineration, comminution	Smelting	Leaching, selective precipitation, electrowinning	Li_2CO_3, Ni, Co, $MnCO_3$		Electrolyte

After thermal treatment at 670 °C in inert and 720 °C in air atmosphere Cu was concentrated in a coarse fraction (> 425 µm), that also was the densest and probably possible to separate by gravimetrical methods. Most of the graphite was found in the two finer fractions 38-100 µm and < 38 µm of the BM, 13-39 % and 19-20% of graphite, respectively, together with Co, Ni, Mn and Li. Separation of graphite and metal containing phases in these two fractions could be achieved by flotation.

Li and Mn recovery: In some of the processes in **Table 17** Li and Mn are not recovered and will instead become part of the slag and not have a specific use. Co, Ni, and Mn's yields in the investigated process are 98.2%, 98.4%, and 91.5%, respectively, and 68% of Li was successfully directed to the dust. Li in the dust could be leached to up to 77% in lime milk and 93% of leached Li was recovered as $LiOH \cdot H_2O$. This corresponds to an overall yield Li of 49%, which positive, but not sufficient if considering the battery regulation. LiOH is in general preferred as feed in LIB's production. As only a two pilot EAF tests were conducted, it is believed that with additional experiments in lab and in pilot scale, further optimisation to direct more Li to the dust is possible through modification of slag and reducing conditions. Also, there is potential to reach higher leaching efficiencies, and by solution purification prior crystallisation there is potential to achieve sufficient purity.

3 References

[1] H.E. Melin: *In World Economic Forum: Cologny, Switzerland*. 2018, pp. 1-11.

[2] J.A. Ober: *Minerals Yearbook – Lithium*. U.S. Geological Survey, 1994.

[3] B.W. Jaskula: *Minerals Yearbook – Lithium*. U.S. Geological Survey, 2020.

[4] P.K. Choubey, M. Kim, R.R. Srivastava, J. Lee and J. Lee: *Minerals Eng*, 2016, vol. 89, pp. 119-37.

[5] W. Zhang, C. Xu, W. He, G. Li and J. Huang: *Waste Manag Res*, 2018, vol. 36, pp. 99-112.

[6] C. Liu, J. Lin, H. Cao, Y. Zhang and Z. Sun: *J Clean Prod,* 2019, vol. 228, pp. 801-13.

[7] B. Makuza, Q. Tian, X. Guo, K. Chattopadhyay and D. Yu: *J Power Sources*, 2021, vol. 491, pp. 229622.

[8] 8. I. Kayacan and Ö Doğan: Energ Source Part A, 2008, vol. 30, pp. 385-91.

[9] 9. J. Ceamanos, J. Mastral, A. Millera and M. Aldea: J Anal Appl Pyrolysis, 2002, vol. 65, pp. 93-110.

[10] 10. A. Aboulkas and A. El Bouadili: Energy Convers Manag, 2010, vol. 51, pp. 1363-9.

[11] 11. S. Lomakin, I. Dubnikova, A. Shchegolikhin, G. Zaikov, R. Kozlowski, G. Kim and G. Michler: J Therm Anal Calorim, 2008, vol. 94, pp. 719-26.

[12] .W. Bale, E. Bélisle, P. Chartrand, S.A. Decterov, G. Eriksson, A.E. Gheribi, K. Hack, I.-H. Jung, Y.-B. Kang, J. Melançon, A.D. Pelton, S. Petersen, C. Robelin, J. Sangster, P. Spencer, M-A. Van Ende, Reprint of: FactSage thermochemical software and databases, 2010–2016, Calphad, Volume 55, Part 1, 2016, Pages 1-19, ISSN 0364-5916, https://doi.org/10.1016/j.calphad.2016.07.004

[13] X. Hu, E. Mousa, G. Ye, Recovery of Co, Ni, Mn, and Li from Li-ion batteries by smelting reduction -Part II: A pilot-scale demonstration, Journal of Power Sources 483 (2021) 229089

[14] A. Andersson, L.S. Ökvist, Hydrometallurgical Recycling of Lithium from Off-Gas Dust Generated in Pyrometallurgical Treatment of Lithium-Ion Batteries, Proc. Of the 59th annual conf. of metallurgists (COM2020), Electronic proceedings ISBN: 978-1-92687, 2020

[15] 1. O. A. Nasser and M. Petranikova, "Review of Achieved Purities after Li-ion Batteries Hydrometallurgical Treatment and Impurities Effects on the Cathode Performance," *Batteries*, vol. 7, no. 3, p. 60, Sep. 2021, doi: 10.3390/batteries7030060.

[16] 2. Y. Ma, M. Svärd, X. Xiao, J. M. Gardner, R. T. Olsson, and K. Forsberg, "Precipitation and Crystallization Used in the Production of Metal Salts for Li-Ion Battery Materials: A Review," *Metals (Basel)*, vol. 10, no. 12, p. 1609, Nov. 2020, doi: 10.3390/met10121609.

[17] 3. G.A. Moldoveanu, G.P. Demopoulos, Organic solvent-assisted crystallization of inorganic salts from acidic media, Journal of Chemical Technology & Biotechnology. 90 (2015) 686–692. https://doi.org/10.1002/jctb.4355

[18] 4. G. Wypych, Handbook of Solvents-George Wypych-ChemTech-Ventech!, (2001).

[19] 5. Khosravi J (2007). Production of Lithium Peroxide and Lithium Oxide in an Alcohol Medium. Chapter 9: Results. ISBN 978-0-494-38597-5

[20] *REGULATION (EU) 2023/1542 OF THE EUROPEAN PARLIAMENT AND OF THE COUNCIL of 12 July 2023 concerning batteries and waste batteries, amending Directive 2008/98/EC and Regulation (EU) 2019/1020 and repealing Directive 2006/66/EC*. 2023.

[21] Zsolt Dobó, Truong Dinh, Tibor Kulcsár, A review on recycling of spent lithium-ion batteries, Energy Reports, Volume 9, 2023, Pages 6362-6395, ISSN 2352-4847, https://doi.org/10.1016/j.egyr.2023.05.264